Applied Water Science (2025) 15:194
https://doi.org/10.1007/s13201-025-02556-5

ORIGINAL ARTICLE

Effective elimination of indigo carmine in wastewater using green nanostructured modified biochar: optimization, sorption equilibrium, kinetics, thermodynamics and mechanisms

Mai ElKammah[1] · Elsayed Elkhatib[2] · Maneea Moubarak[3]

Received: 13 March 2024 / Accepted: 11 June 2025

Abstract
This research examined the application of nano-activated biochar (nMOSAB) produced from *Moringa oleifera* seeds (MOS) as an adsorbent for the removal of indigo carmine (IC) dye. The synthesis of nMOSAB involved grinding techniques combined with thermal pyrolysis at temperatures exceeding 600 °C, resulting in the formation of nano-sized biochar particles. The adsorption data were evaluated using the Langmuir model for equilibrium and the pseudo-second-order model for kinetics. The nano-biochar exhibited a maximum adsorption capacity of 344.8 mg g^{-1}. In comparison with bulk biochar particles, the adsorption capacity of nMOSAB was found to be 9.5 times greater. The high adsorption capacity can be attributed to various chemical interactions during the adsorption process, such as π–π interactions, hydrogen bonding, and electrostatic interactions. Thermodynamic analyses indicated that the adsorption process is both spontaneous and exothermic. Through traditional batch tests and a packed-bed system, the effectiveness of nMOSAB for the removal of IC from actual wastewater was determined to be 91.6% and 89.6%, respectively. This research clearly demonstrated the capability of nano-biochar derived from *M. oleifera* seeds to serve as an efficient, eco-friendly, and economical adsorbent for the removal of IC dyes from wastewater.

Keywords Adsorption · Indigo carmine · *Moringa oleifera* · Nano-biochar

Introduction

One of the main contributors to environmental contamination issues is the use of synthetic dyes and pigments in a variety of aspects. Many industries rely mainly on the contribution of different dyes during the operation of production, such as the manufacture of paper, plastics, cosmetics, leather, and textiles pigmenting (Li et al. 2020). Additionally, these industries' effluents include high levels of suspended organic particles and hazardous byproducts that are non-biodegradable, which could cause harmful damage to the ecosystem (Jamil et al. 2024).

Indigo carmine is an anionic dye and contributes to many pharmaceutical applications (Tabti et al. 2022) and textile industries, especially denim dying (Choi 2021). There is a growing interest in the removal and treatment of wastewater to mitigate the toxic effects of industrial chemicals, addressing the challenges associated with wastewater management and ensuring safe disposal (Behera et al. 2021).

The treatment of dye effluents originating from industrial and commercial discharges has extensively employed methods such as advanced oxidation processes, membrane separation, and electrochemical degradation, all of which have demonstrated their effectiveness in wastewater treatment. Adsorption techniques using waste materials as sorbents are one practical and promising easy applied approach (Sikdar et al. 2020; Gallego-Ramírez et al. 2024). The ability

✉ Elsayed Elkhatib
selkhatib1@yahoo.com

Mai ElKammah
mai_elkammah@agr.dmu.edu.eg

Maneea Moubarak
drmaneea1981@agr.dmu.edu.eg

[1] Department of Natural Resources and Agricultural Engineering, Faculty of Agriculture, Damanhour University, Damanhour 22511, Egypt

[2] Department of Soil and Water Sciences, Faculty of Agriculture (El-Shatby), Alexandria University, Alexandria 21545, Egypt

[3] Department of Horticulture, Faculty of Agriculture, Damanhour University, Damanhour 22511, Egypt

Published online: 05 July 2025

of reusing sorbents over a number of cycles gave them the character of sustainability and feasibility for dye removal from effluents (da Silva et al. 2020; Hynes et al. 2020).

Biochar is produced through the thermochemical conversion of waste biomass and serves as a means for sequestering various emerging contaminants in wastewater treatment (Sambo et al. 2024). This carbon-rich material possesses a microporous structure and a considerable specific surface area, enhancing its efficacy and applicability relative to other sorbents (Jindo et al. 2014; Abbey et al. 2023). The production of biochar depends on the pyrolysis of agricultural wastes and organic solid wastes applying low oxygen levels and high temperature (< 700 °C) (Lehmann and Joseph 2015; O'Connor et al. 2018; Wang et al. 2020a). Biochar can be created from several bio- mass sources accordingly, the chemical and physical characterization affected by its parent material (Wang et al. 2020b). Biochar porously nature and its containment of certain amount of enrich functional groups which includes alkyl, aromatic, hydroxyl (–OH), and carboxyl (–COOH) groups have enhanced its ability for elimination of several pollutants and to interact with organic and inorganic compounds, facilitating their degradation or immobilization (Shakoor et al. 2020; Zhang et al. 2020).

The continued exploration of advanced nanomaterials holds great potential for further advancements in technology and innovation. Nano-biochar has gained remarkable curiosity in the scientific research due to its enhanced chemical properties represented in large expanse of area, long-term durability, eco-friendly and the most important reason is that nano-biochar holds the characteristics of nanomaterials and biochar together (Shaikh et al. 2020).

Moringa oleifera seeds (MOS) have been used in negligible studies as bio-sorbent for dyes caption (Akhtar et al. 2007; Beltrán-Heredia and Sánchez-Martín 2008; Beltrán-Heredia et al. 2009). El-Kammah et al. (2022a) has tested the adsorption capacity of nanoparticles derived from MOS after extracting the oily contents for IC uptake.

In this study, further experiments were carried out to develop a nanostructured activated biochar derived from *M. oleifera* seeds and investigate for the first time its capability for elimination IC dyes from textile wastewater.

Experimental methods

Preparing of activated biochar derived from *Moringa oleifera* seeds (MOSAB)

The seeds of *M. oleifera* were acquired from Egyptian local markets. Oily seeds were treated with organic solvents to extract essential oil, and then, the non-oily product was dried at 60 °C. The partially dried samples were passed through 2 mm sieve. Passing powder was collected and fed into a muffle furnace to be pyrolyzed at 600 °C for 3 h. According to Bagheri et al. (2020), biochar was let to be cool and then mixed with phosphoric acid (85 wt% H_3PO_4) for chemical activation. Activated MOSB was dried over night at 40 °C and then passed into 45 µm sieve. Passing particles were grinded with planetary ball mill to diminish the particles size less than 100 nm following Elkhatib technique (Elkhatib et al. 2015). The fraction with size > 100 nm was collected and labeled as nano-*Moringa oleifera* Seeds Biochar (nMOSAB).

Characterization of activated nano-biochar

Some analytical characterization involved elemental contents and features were determined for nMOSAB before and after capturing IC dye using scanning electron microscope (SEM) conjunction with energy-dispersive X-ray spectroscopy (EDX)—JSM-IT200 Series (Oxford Instruments, UK). The FTIR spectroscopy analysis was carried out to gain insights into the surface chemistry of functional groups present on the nMOSAB by utilizing the PerkinElmer Model 400 apparatus. The nanoparticle tracking analysis (NTA) for *M. oleifera* biochar was conducted using the ZetaSizer Nano ZS (Malvern Panalytical) as illustrated in Fig. S2. The size of each particle is calculated based on the velocity of its movement.

The zero point of charge of nMOSAB was evaluated to understand biochar's surface properties and evaluate the biochar's surface charge density. The method utilized for estimation the pH_{ZPC} was reported by Kosmulski (2009) and summarized in combining (0.2 g) of the sorbent material with a level of sodium chloride solutions (0.01 M) to achieve specific pH values starting from 2 to 10 through altering the acidity or alkalinity levels by adjusted acidic or alkaline solutions. The shaken period for mixture components was 24 h. The final pH values for each solution were measured. The graph of pHzpc was represented by plotting the relationship between initial pH values against the disparity between the starting and final pH values (Fig. 6). The depicted line's intersection with the original pH axis is known as the pHzpc.

Indigo carmine

Indigo carmine (IC) is a negatively charged dye with a molecular weight of 466.35 g per mole. The IC was bought from ANALEMA (Vigo, Spain) and had a purity of 99%. Concentrated synthetic stock solution (1000 mg/L) from pure IC was prepared with deionized water and kept in fridge at 4 °C in darkness. Daily working solutions were freshly diluted from the IC stock solution with deionized water. The determination method involves using spectroscopic techniques and is described in supplementary material. Additionally, the chemical characteristics of IC dye, such as

its solubility, stability, and reactivity, are also described in supplementary material (Fig. S1).

Adsorption experiments

The batch adsorption experiments of indigo carmine dye on bMOS and nMOSAB were carried out by mixing 0.1 g of the adsorbents with 10 ml of IC solution in 50-ml polypropylene centrifuge tubes. The mixtures were agitated at 160 rpm at 25 °C for varying time periods ranging from 5 min to 24 h to determine the equilibrium conditions. The centrifugation process was carried out for five minutes on the suspensions at 4000 rpm (1800 g) to separate the precipitate containing the adsorbent materials. The filtration process consisted of filtering the mixture through 0.45-micron Millipore filter papers. These filter papers trapped the solid particles while permitting the liquid supernatant to go through. The UV–Vis spectrophotometry technique was employed to assess the concentration of residual dye in supernatant solutions. Both IC removal percentage (%) and IC adsorbed quantity (mg g^{-1}) were computed using the equations presented in supplementary material.

To provide valuable insights into the behavior of nMOSAB and its interactions with the dye molecules, various mathematical models were applied to identify the trends in adsorption isotherms (Table 1) and kinetics (Table 2).

Statistics

All adsorption experiments were repeated three times. The mean of the three replicates was used to report all experimental data. The standard error of the mean was calculated and represented through error bars. The linear least squares regression method was used in Microsoft Excel to plot the data gathered from previous experiments.

Results and discussion

Characterization of nMOSAB

SEM analyses

The surface morphological structure of activated biochar before and after IC sorption is represented in Fig. 1. The micrograph of nMOSAB revealed multiple cavities distributed over rough external surface. Uneven pores and nanosized spherical shapes were noticed (Fig. 1A) (Mashhadimoslem et al. 2021). Several high temperatures treated sorbents appeared similar surface characteristics including the existence of pore structure which returns to the breakdown of the lignocellulosic material (Bello et al. 2017). After loading with dye particles onto the biochar,

Table 1 Adsorption isotherms models for the adsorption of indigo carmine by nMOSAB and bMOS

Adsorption isotherms	Description	Parameters	Adsorbent	
			nMOSAB	bMOS
Freundlich $q_e = K_F C_e^{1/n}$	K_F = constants of Freundlich (the adsorption volume of the adsorbent) $1/n$ = constants (intensity of the analyte adsorption)	K_F (mL/g) $1/n$ R^2 SE	1.9074 0.9048 0.9895 0.1351	0.1339 0.9602 0.9975 0.0881
Langmuir $q_e = \frac{q_{max} K_L C_e}{1+K_L C_e}$	q_{max} = maximum adsorption capacity K_L = constant of Langmuir (free energy of adsorption)	q_{max} (mg/g) K_L (L/mg) R^2 SE	344.8 0.0195 0.9986 0.0078	36.10 0.0432 0.9908 0.0062
Temkin $\theta = \frac{RT}{\Delta Q} \ln K_0 C_e$	ΔQ = variation of adsorption energy ($-\Delta H$) K_0 = constant of Temkin T = temperature (K) R = universal gas constant	ΔQ (J/mol) K_0 (L/mg) R^2 SE	39771.98 1.3971 0.8467 0.0278	10144.63 0.34946 0.9847 0.05433
Fowler–Guggenheim (FG) $K_{FG} C_e = \frac{\theta}{1-\theta} \exp\left(\frac{2\theta W}{RT}\right)$	W = interaction energy between adsorbed molecules K_{FG} = constant of Fowler–Guggenheim θ = fractional coverage	W (J/ mol) K_{FG} (L/mg) R^2 SE	4749.76 39.1617 0.9648 0.1869	859.6468 31.84244 0.4469 0.2946
Kiselev $K_K C_e = \frac{\theta}{(1-\theta)(1+K_n \theta)}$	K_K = constant of Kiselev K_n = constant (complex formation between adsorbed molecules)	K_K (L/g) K_n R^2 SE	0.0195 0.1435 0.9965 0.054	0.0059 9.694 0.8971 0.0377
Hill–de Boer $K_1 C_e = \frac{\theta}{1-\theta} \exp\left(\frac{\theta}{1-\theta} - \frac{K_2 \theta}{RT}\right)$	K_1 = constant of Hill-de Boer K_2 = constant (interaction between adsorbed molecules)	K_1(L/mg) K_2 (J/mol) R^2 SE	48.41453 2003.86 0.1833 0.1154	82.1708 8030.892 0.7893 0.2049

Table 2 Adsorption capacity of various absorbents for removal of some anionic dyes in aqueous effluents

Sorbents	Maximum adsorption capacity	
Acacia nilotica (babool) sawdust activated carbon	4.8 ($mg{\cdot}g^{-1}$)	(Gupta and Lataye 2017)
pristine carbon nanotubes (PCNTs)	93 ($mg{\cdot}g^{-1}$)	(Elamin et al. 2023)
zinc oxide green pea peels biochar nanocomposite ZnO/ GPBC	114.94 ($mg{\cdot}g^{-1}$)	(Rubangakene et al. 2023)
innovative green pea peels biochar (GPBC)	62.11 ($mg{\cdot}g^{-1}$)	(Rubangakene et al. 2023)
nano-Magnetic Sophora Japonica Fruit Seed Biochar	434.783 ($mg{\cdot}g^{-1}$)	(Bayram et al. 2022)
Sophora Japonica Fruit Seed Biochar	76.923 ($mg{\cdot}g^{-1}$)	(Bayram et al. 2022)
Nanocomposite hydrogels	370.37 ($mg{\cdot}g^{-1}$)	(Dalaran et al. 2011)
Carbonaceous material from pyrolyzed sewage sludge	92.83 ($mg{\cdot}g^{-1}$)	(Gutiérrez-Segura et al. 2009)
Commercial Activated carbon	298.34 ($mg{\cdot}g^{-1}$)	(Harrache et al. 2019)
Nanofiber membranes	266.77 ($mg{\cdot}g^{-1}$)	(Li et al. 2012)
Moringa oleifera Seed Extract	343 ($mg{\cdot}L^{-1}$)	(Beltrán-Heredia et al. 2009)
Nano-Moringa oleifera seeds Activated Biochar (nMOSAB)	344.8 ($mg{\cdot}g^{-1}$)	This work
Bulk Moringa oleifera seeds (bMOS)	36.1 ($mg{\cdot}g^{-1}$)	This work

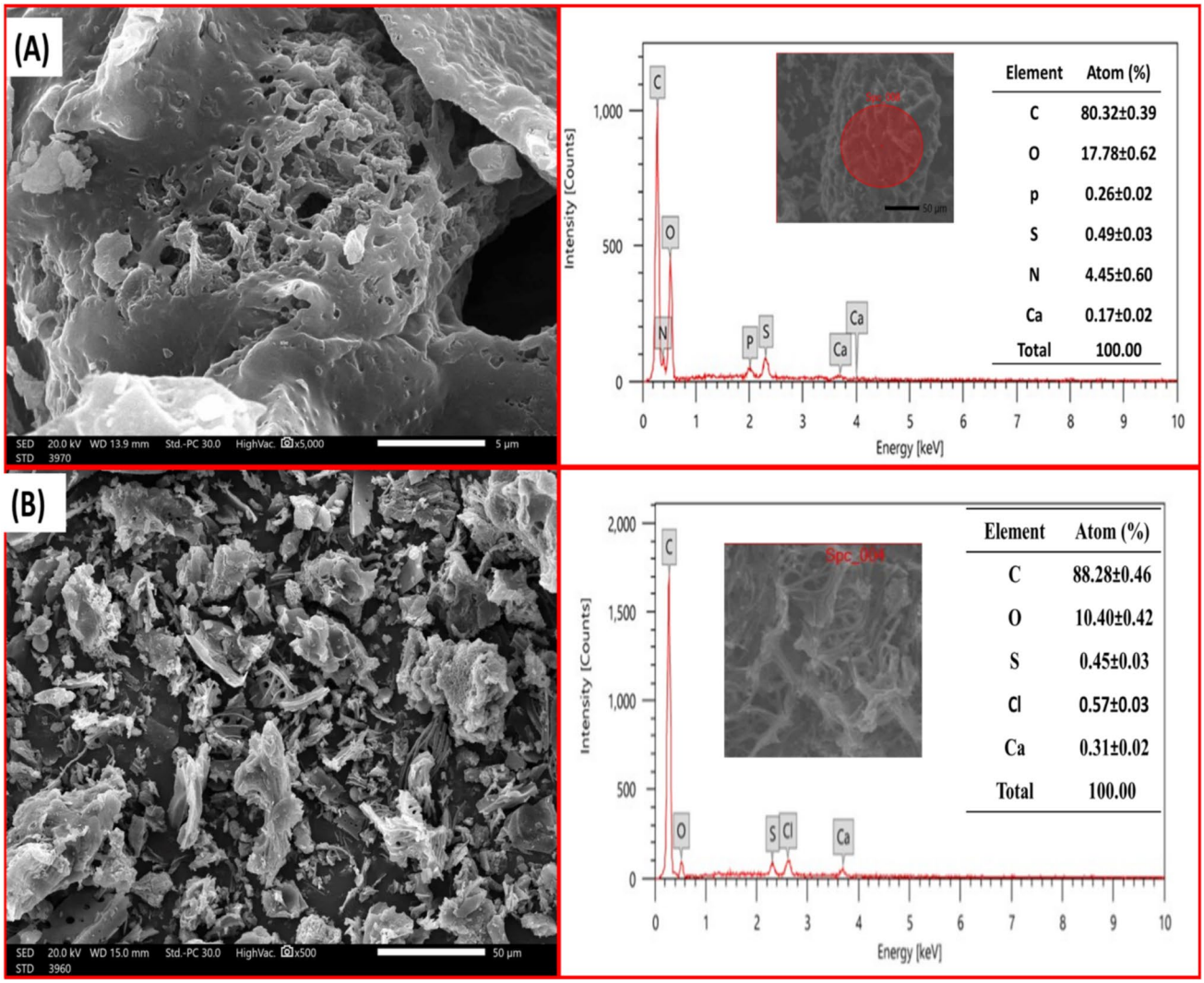

Fig. 1 SEM–EDS analysis of **A** nMOSAB and **B** IC loaded nMOSAB

agglomerated layers were observed onto biochar surface and the distribution of pore sizes has changed (Fig. 1B).

EDS elemental analysis

The chemical composition of the sorbent material is determined through elemental distribution analysis. This technique identifies the types of chemical elements present and their relative abundance in the material. The elemental analysis results are presented in Fig. 1. For bare nMOSAB, high percentage of carbon (80.32%) and moderate percentages for oxygen and nitrogen (17.87% and 4.45%), respectively, were spotted. Remarkably low concentration of phosphorus, sulfur and calcium was noticed, whereas, after IC adsorption, the elemental analysis showed an increase in carbon percentage (88.28%) which confirms the interaction of the activated biochar with IC functional groups and exposing soluble base ions (such Na^+, K^+, etc.) on nMOSAB surface. The decrease in O ions percentage from 17.87 to 10.40% suggested the contribution of O ions in the adsorption process.

Nanoparticles tracking analysis of nMOSAB

The analysis of biochar nanoparticles revealed a distinct size distribution curve characterized by a pronounced peak at 60 nm, with a narrow size range of 50–80 nm, as illustrated in Fig. S2. The methods employed in biochar production, including pyrolysis and activation, can effectively regulate the variation in particle size, resulting in more uniform particles that possess a high surface area, thereby enhancing the adsorption efficiency. In a prior study, the specific surface area of nano-Moringa oleifera seeds was reported to be 4.6 $m^2\ g^{-1}$ (El-Kammah et al. 2022a).

The FTIR spectroscopy of nMOSAB

A sharp and active band at 3727 cm^{-1} was observed in FTIR analysis spectra of *nano-Moringa oleifera* seeds (nMOS) prior adsorption indicating its role in the interactions contributing to removal processes (Fig. 2). This band refers to the O–H bond stretching vibration mainly existing in proteins, lignin, carbohydrates and fatty acids. The band around 2977–2871 cm^{-1} is attributed to the aliphatic C–H group according to (Feng et al. 2011). The band seen at 1571 cm^{-1} is associated with the C=O stretch, while the bands from 1232 to 1165 cm^{-1} match the $–SO_3$ stretching vibration (Chaari et al. 2019).

After IC adsorption, new changes in the frequency of the functional groups and peak intensity were noticed. These changes indicate the role of the aforementioned functional groups of biochar in adsorption of IC dye. The shift in the peak at 3727 cm^{-1} to a lower wavelength of 3697 cm^{-1} suggests a change in the O–H groups' existence on the nMOSAB surface during IC adsorption. This shift was accompanied by an increase in the width of the band which provides further evidence of the involvement of OH groups in the adsorption process. The reduction in intensity of the peak at 1571 cm^{-1}, corresponding to C–H groups, highlights the significant role of these functional groups in capturing reaction performance (Araújo et al. 2010, 2013).

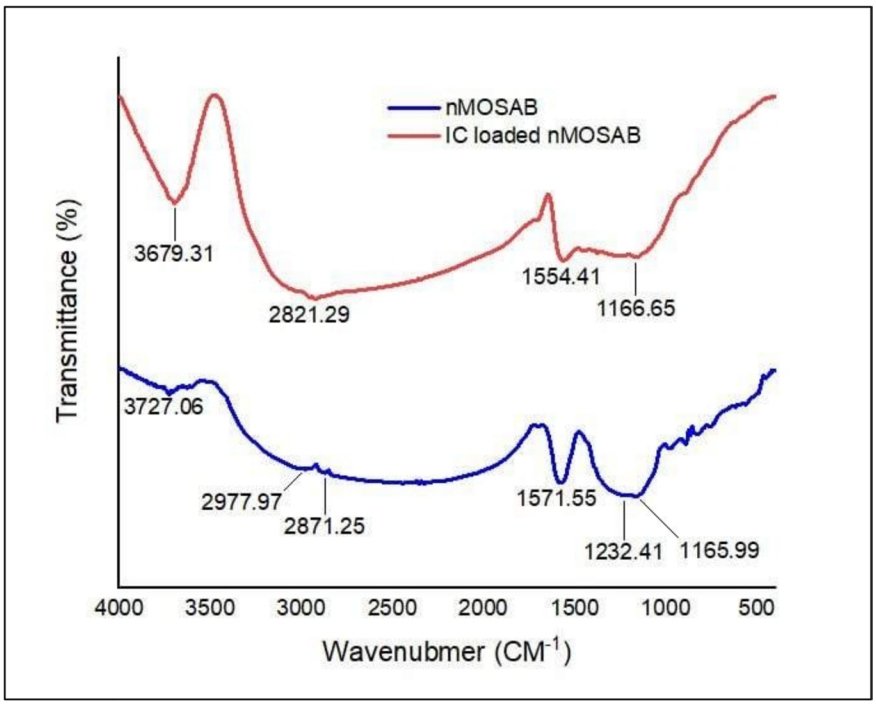

Fig. 2 FTIR spectra of nMOSAB (lower) and IC loaded nMOSAB (upper)

Adsorption equilibrium

Adsorption isotherms are utilized to describe the adsorption performance and hypothesis, providing information about the affinity between sorbents and the surrounding media at equilibrium (Elkhatib et al. 2017, 2024). The IC adsorption isotherms models are shown in Table 1 with their calculated parameters (El-Kammah et al. 2022a). Langmuir isotherm was the best model to describe IC adsorption data onto nMOSAB and bMOS as evidenced by the very low standard error (SE) (Table 1). The H-type sorption isotherm of nMOSAB (Fig. 3A) indicates the high affinity between dye molecules and biochar surface, and the best fit to Langmuir model predicts the homogenous nature of biochar surface with monolayer sorption of dye molecules onto biochar active sites (Fito et al. 2023; Oyekanmi et al. 2024).

The maximum adsorption capacity of IC on nMOSAB was determined to be 344.8 mg g^{-1}, which represents an increase of 9.5 times in comparison with the bulk MOS. Table 2 lists the maximum adsorption capacity (q max) of various adsorbents for the elimination of IC anionic dye from aqueous solutions. It is evident that the nMOSAB absorbent performed much better than most of the adsorbents on the list.

Optimum parameters of indigo carmine adsorption onto nMOSAB

Contact time

In order to define an efficient and economical adsorption for IC onto biochar, specified contact time for the adsorption process was determined. The influence of agitation time for different time intervals (1 min–24 h) was assessed. For the first five minutes, the IC got absorbed quickly and then slightly increased until it approached the equilibrium phase. The greatest indigo carmine elimination efficiency percentage was 97.5% after 90 min (Fig. 4A). High adsorption capacity in the first 20 min could be due to the abundance of vacant active sites onto nMOSAB. As the interaction between dye molecules and surface-active site growing up, most of the active sites become occupied and the remaining

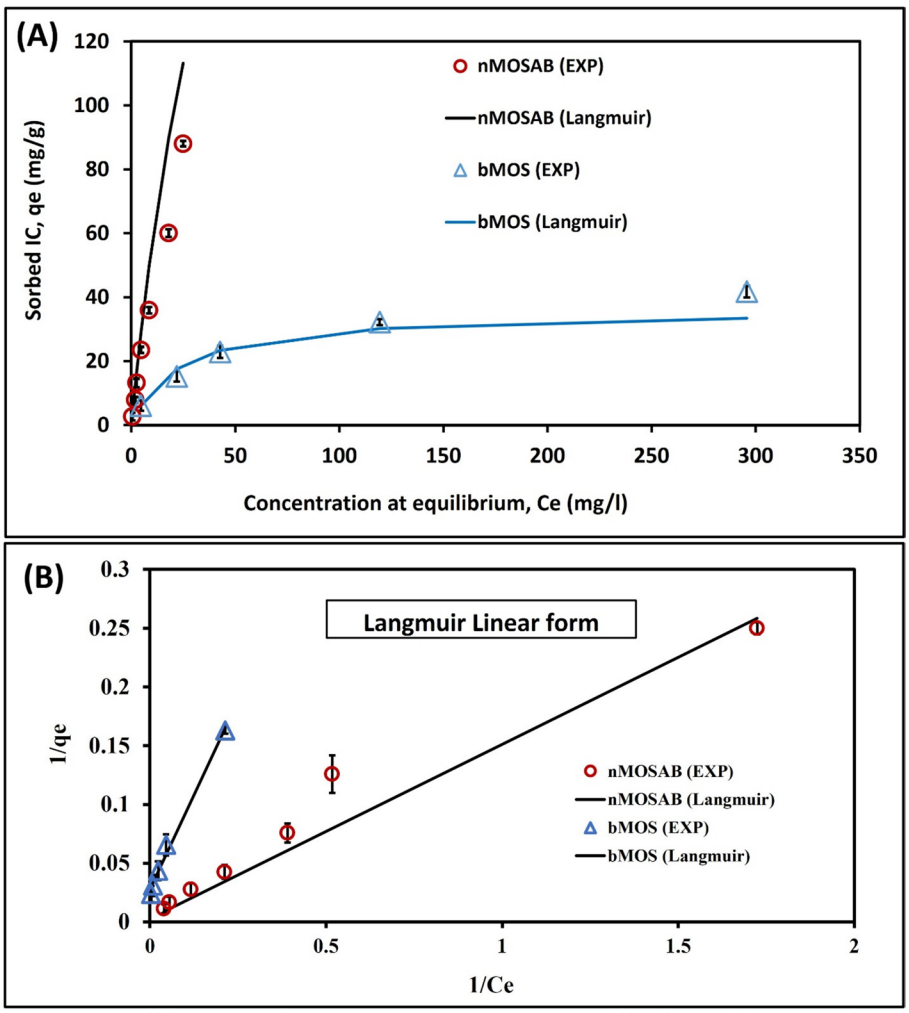

Fig. 3 Adsorption isotherm **A** The nonlinear form of Langmuir model for IC adsorption by bMOS and nMOSAB **B** The linear form of Langmuir model for IC adsorption by bMOS and nMOSAB. Error bars represent the mean of standard error

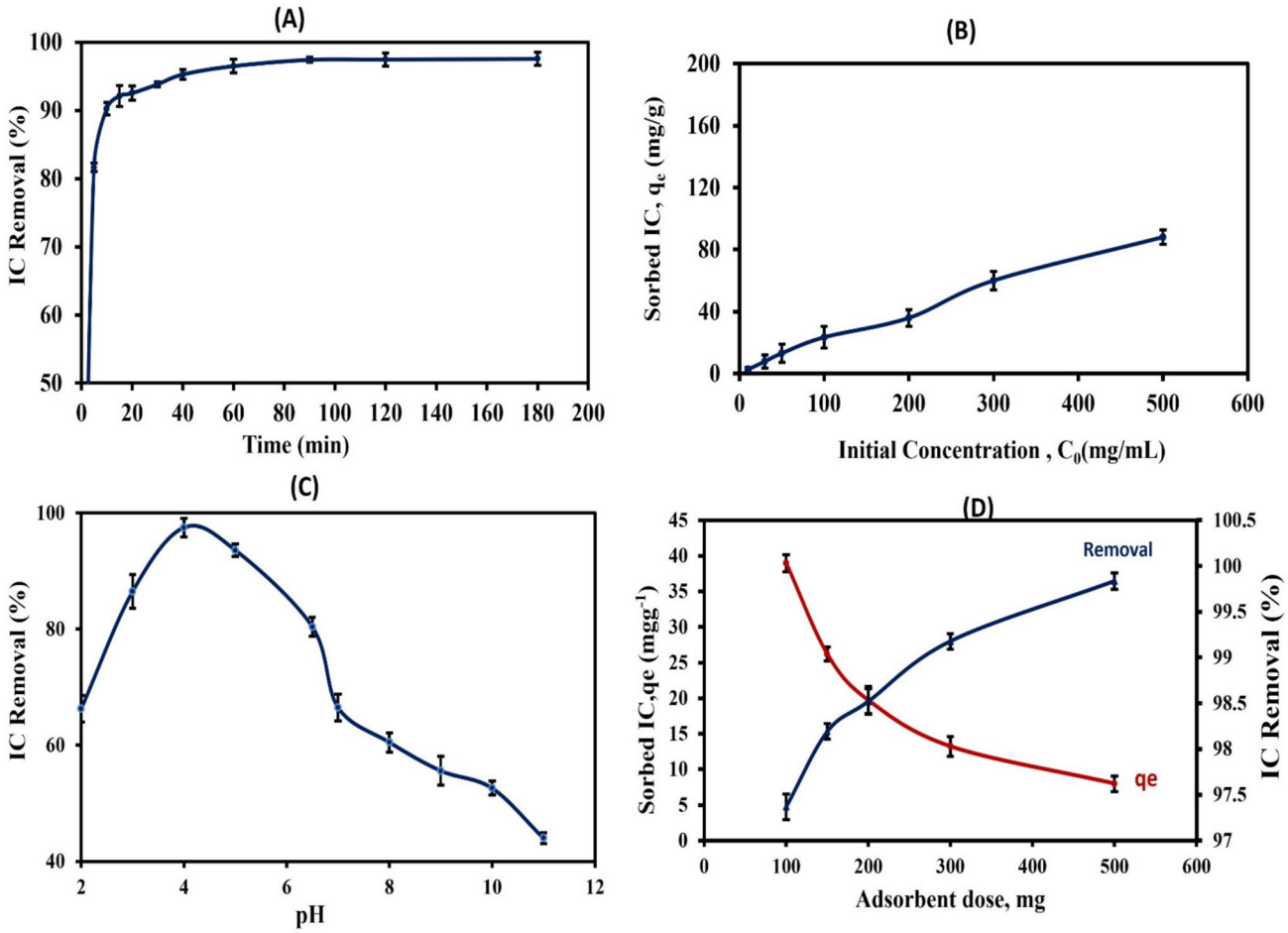

Fig. 4 Adsorption of IC in nMOSAB. Effect of **A** contact time, **B** initial IC concentration, **C** solution pH, and **D** adsorbent dose. Error bars represent the standard error of mean

limited numbers of adsorption sites were insufficient to capture dye molecules (Singh and Choden 2016; El-Maghrabi et al. 2024).

Indigo carmine (IC) initial concentration

To determine the optimal IC dye concentration, various experiments were conducted to measure the adsorption capacity at different concentrations using 100 mg of nMOSAB with a series of dye initial concentration from 10 to 500 mg L^{-1}, while other parameters were maintained. The results plotted in Fig. 4B showed gradual increase in nMOSAB adsorption capacity with the increase in IC initial concentration. It is proposed that the concentration of IC acts as a catalyst, causing more dye molecules to migrate from the solution to the adsorbent surface (Keerthana Devi and Geethakarthi 2022). This result is concordant with the previous studies reported by other investigators (Ferreira et al. 2019; El-Kammah et al. 2022b, a).

The pH effect and point of zero charge (PZC).

Solution pH has a significant influence on adsorption due to its effect on both the sorbent material outer charge and the ionization degree of the adsorbate species (Das and Jana 2006; de Oliveira Brito et al. 2010). The effect of dye solution pH on IC adsorption by nMOSAB was examined through various tests at different pH values from 2 to 11, and the results are plotted in Fig. 4C. The findings showed greater adsorption capabilities at moderately acidic pH levels. The highest removal percentage (97.5%) of IC by nMOSAB was achieved at pH value 4. In contrary, increasing pH values above 7 has a profound effect on *reducing* the amount of amount of IC removed by nMOSAB. These findings were consistent with adsorption of anionic dye (Congo Red dye) onto calcium rich biochar (Dai et al. 2018). These results can be attributed to the theory of pHpzc which provides insights to understand the surface chemistry of nano-sorbents and adsorption behavior of substances onto sorbent surface.

The pHpzc of nMOSAB was evaluated and found to be 6.8 (Fig. 5) which suggests the presence of variable electrostatic charges at different pH levels. It is therefore expected that at pH < pHpzc nMOSAB nanoparticles will acquire positive charges on the external surfaces and the negatively charged IC dominates. In contrary at pH values > pHpzc electrostatic repulsion takes place and the rate of adsorption process is reduced (Gadekar and Ahammed 2020; Sahnoun et al. 2024). Similar result was reported for *M. oleifera* biochar (Bagheri et al. 2020).

Adsorbent dose

The effect of adsorbent dose on the adsorption capacity and the rate of adsorption is a crucial factor to consider in the removal process (Nodeh and Sereshti 2016). The impact of nMOSAB adsorbent dosages ranging from 100 to 400 mg on limitation dye efficiency was explored with IC dye solution of 100 mg g^{-1}. It was found that increasing adsorbent dosage from 100 to 500 mg diminished nMOSAB adsorption capacity from 38.9 to 7.9 mg g^{-1} with simultaneous increase in the IC removal efficiency from 97.3 to 99.8% (Fig. 4D). It was obvious that increasing the sorbent dose above the weight of 100 mg did not improve the adsorption process. This could be attributed to the overcrowding of adsorption sites due to the clustering of sorbent nanoparticles leading to limiting the accessibility of target molecules. Furthermore, the agglomeration of nanoparticles at higher doses might result in the formation of larger clusters, reducing the surface area available for adsorption (El-Maghrabi et al. 2024). Similar findings for IC removal have approved the same adsorption behavior (Gutiérrez-Segura et al. 2009; Dey et al. 2022).

Adsorption kinetics study

Indigo carmine adsorption kinetic behavior onto nMOSAB was examined at various time intervals (Fig. 6). The adsorption rate raised rapidly within 20 min and then tended to slow down. Adsorption equilibrium was stabled at 90 min recording 97% dye removal efficiency. Five kinetic models were used to simulate the adsorption kinetics data (Elkhatib et al. 2013). These models and their corresponding parameters are described in Table 3. The precise model that could accurately reproduce the findings was identified based on the highest determination coefficient (R^2) and low standard error (SE) values of these models. Kinetics experimental data for IC adsorption onto nMOSAB were best fitted by power function model followed by pseudo-second-order kinetic model (Table 3, Fig. 6). Similar findings were reported by (Saxena et al. 2020) who described anionic dyes capturing onto activated biochar (Fig. 7).

Sorption thermodynamics

Studying sorption thermodynamics is important to explicitly assess the impact of temperature on adsorption efficiency. Calculation of thermodynamics parameters are detailed in supplementary material. The parameters of thermodynamics were established and are documented in Table 4. The negative values of $\Delta G°$ observed at the three temperatures indicate that the adsorption process of IC is spontaneously favorable (Ho et al. 2000). Additionally, the percentage of IC dye removal from the solution decreased from 96.8 to 78.5% as the temperature increased. This aligns with the rising $\Delta G°$ values, which suggest a reduction in spontaneity at elevated temperatures, thereby confirming the unfavorable nature of IC capturing under such conditions (Blanco et al. 2017). The

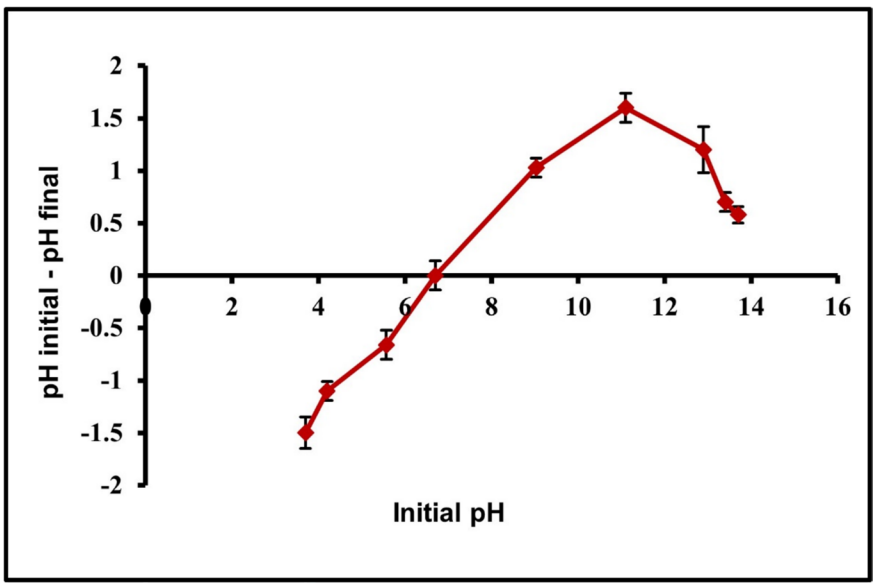

Fig. 5 pH of point of zero charge (pH_{PZC}) for nMOSAB adsorbent material

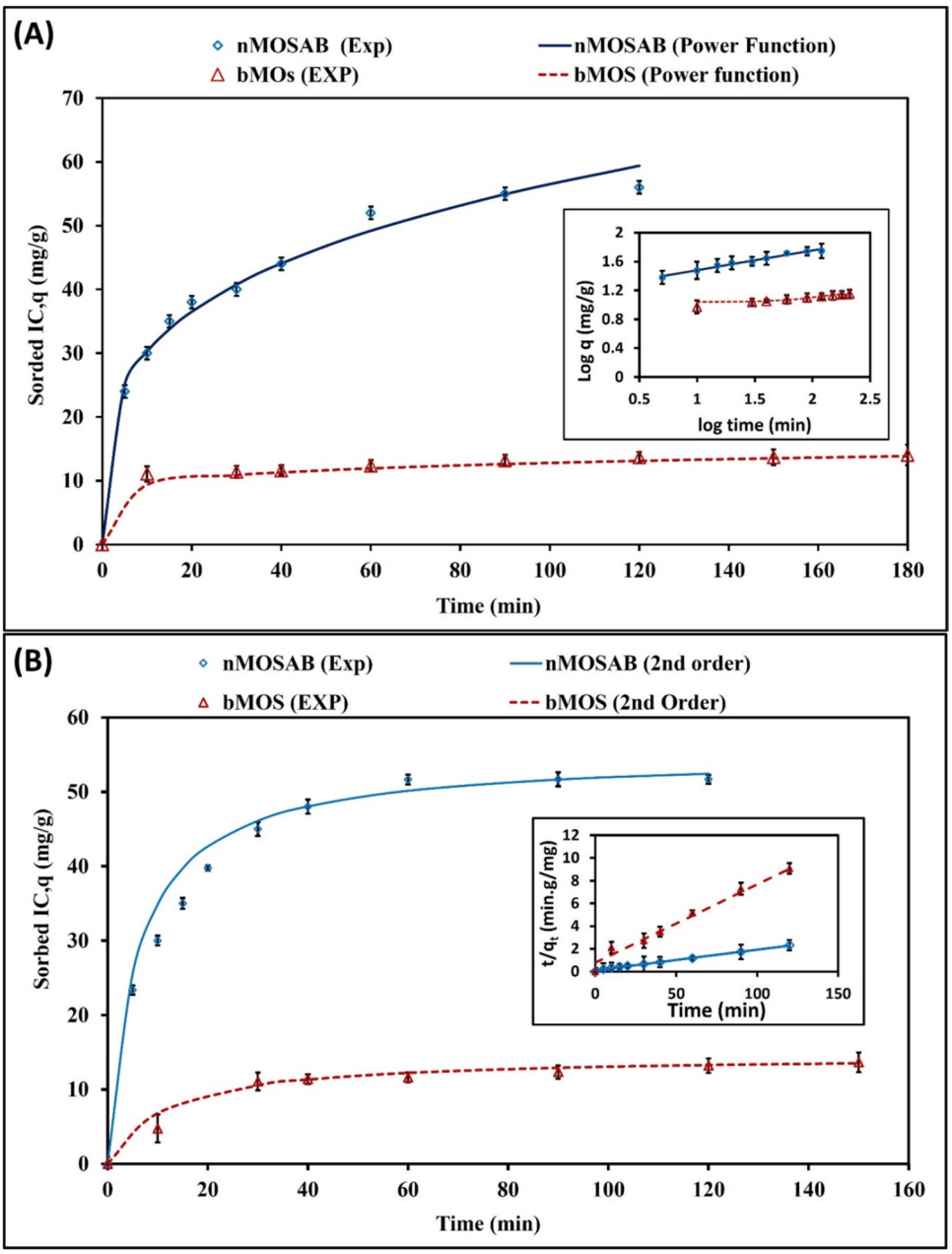

Fig. 6 Adsorption kinetic models, **A** Power function model and, **B** Pseudo-second-order model for biochar nanoparticles and bulk particles of Moringa seeds, the inset shows the linear forms of the models. Error bars represent the mean of standard error

adsorption process is exothermic according to the negative value of $\Delta H°$. System randomness was inferred from the positive value of entropy which reflects that the system is in the state of disorder without altering in internal structure of nano-biochar. The same interaction nature was indicated with silver nanoparticles biochar in removing textile anionic dyes (Shaikh et al. 2021).

Probable adsorption mechanisms

Adsorption performance of activated biochar could be attributed to the surface chemical characteristic as well as pore structure of the adsorbent (Ullah et al. 2022). The FTIR spectroscopy procedure was utilized to consider the interaction between the adsorbates and active groups on the adsorbent surface. The elucidation of the FTIR is based on the chemical structure of the biochar before and after loading with IC. Vanishes or shifts of FTIR peaks illustrate association of the adsorbates with functional groups on adsorbents surface. The combined effects of multiple factors on adsorption such as π–π conjugation, electrostatic attraction, pore filling and hydrogen bonding force interplay with each other to regulate and determine the overall efficiency of an adsorption system (Sun et al. 2021) as follows:

Table 3 Kinetic model constants, determination coefficients, and standard error of estimate for IC adsorption by nMOSAB and bMOS

Adsorption kinetic model	Description	Parameters	Adsorbent	
			nMOSAB	bMOS
Elovich $q_t = \frac{1}{\beta}\ln(1+\alpha\beta t)$	β = constant related to the extent of surface coverage α = the initial adsorbed rate	α (mg g^{-1} min^{-1}) β (mg g^{-1}) R^2 SE	25.14 0.1030 0.9446 2.624	48.3055 3.0485 0.8738 0.1078
First order $\ln(q_e - q_t) = b - k_1 t$	q_t = amount of IC adsorbed at time t q_e = amount of IC adsorbed at equilibrium K_1 = apparent adsorption rate coefficient b = constant	K_1 (min^{-1}) b (mg/g) R^2 SE	0.0512 3.968 0.8106 0.3368	0.0011 3.8108 0.4412 0.0498
Second order $q = q_e\left[1 - \frac{1}{1+k_b t}\right]$	K_b = apparent adsorbed rate coefficient	K_b (g mg^{-1} min^{-1}) q_e (mg g^{-1}) R^2 SE	0.00315 54.945 0.996 0.0489	0.0060 14.53 0.9942 0.4102
Parabolic diffusion $q_t = a + k_d t^{1/2}$	k_d = apparent diffusion rate coefficient a = constant	k_d (mg/g $min^{-1/2}$) a (mg/g) R^2 SE	2.415 26.56 0.725 5.739	0.727 7.406 0.5665 1.999
Power function $q = k_p C_0 t^{1/m}$	k_p = apparent adsorbed rate coefficient $1/m$ = constant C_0 = initial concentration of IC	k_p (min^{-1}) $1/m$ R^2 SE	16.16 0.2719 0.9822 0.0177	3.152 0.2995 0.7836 0.0727

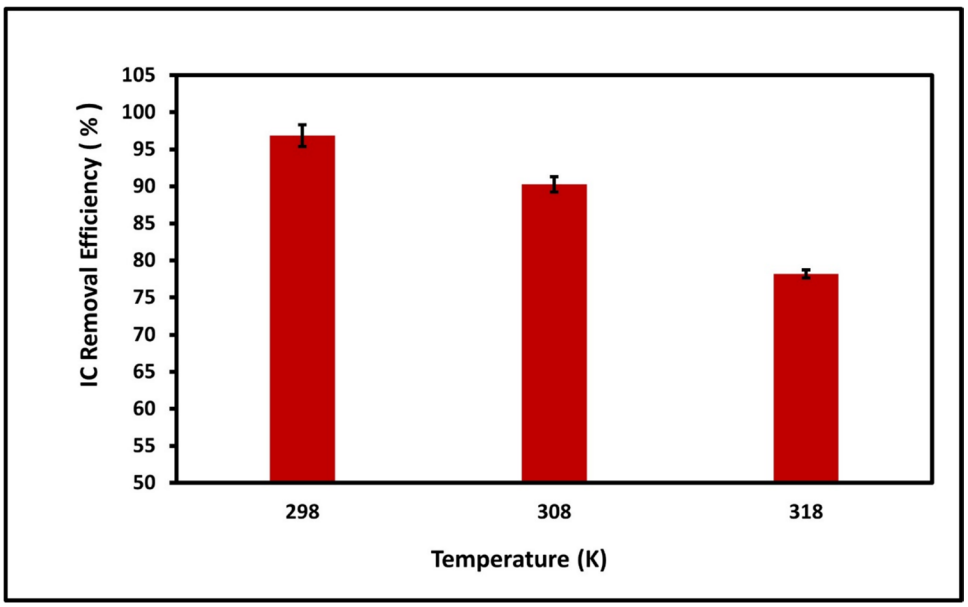

Fig. 7 Influence of temperature on adsorption removal efficiency of IC in nMOSAB at different temperatures (298–318) K

Table 4 Thermodynamics parameters for IC adsorption onto nMOSAB

Adsorbent	Initial IC concentration (mg/L)	T (K)	ΔG^o (kJ/mol)	ΔS^o (kJ/mol K)	ΔH^o (kJ/mol)
nMOSAB	100	298	− 8481.17	255.27	− 84477
		308	− 5702.23		
		318	− 3375.72		
	30	298	− 2513.91	43.245	− 15365
		308	− 1972.03		
		318	− 1649		

1- π–π conjugation: The FTIR spectra represented a substantial shift in the wavelength 1871 cm^{-1} which may be attributed to the creation of the π-π conjugation between the π electron cloud of dye benzene ring and π electrons on biochar surface (Figs. 2 and 8).
2- Hydrogen bonding: Formation hydrogen bonds between dye and functional groups of activated biochar has the potential to enhance the efficiency of adsorption process (Mariska et al. 2024). It is noticeable in the FTIR spectra (Figs.2 and 8) that O–H and N–H peaks assessed significant change due to the existence of hydrogen bonds between nMOSAB –OH groups which serve as (H acceptors) and dye oxygen (-O), benzene rings which act as hydrogen-bonding donners (Zhang et al. 2019).
3- Electrostatic interactions: Electrostatic interactions have been demonstrated as a contributor in the adsorption performance (Fig. 8). Adjusting the pH of dye solution can influence the type of charge that formats onto biochar surface. At low pH degree pH < pHpzc, biochar molecules carry a positive charge, while anionic IC dye is negatively charged. Electrostatic linkage can be enhanced due to the difference between materials charges. Moreover, anionic IC dye ions react with the protonated amino groups, protonated hydroxyl groups and SO_3 of nMOSAB due to (Kekes and Tzia 2020).

Reusability of nMOSAB

To increase the economic feasibility of the treatment procedure, adsorption–desorption cycle was performed to evaluate nMOSAB reusability and stability. Five regeneration tests were carried out using 0.1 g of nMOSAB mixed with 20 ml of IC dye solution under agitation time of 120 min. After centrifuging the suspension, the concentrations of residual IC in the supernatant solution were measured. Adsorbed IC molecules were discarded from the sorbent using 20 ml of deionized water; then, the sorbent was used again in the adsorption tests.

Experimental results figured out in Fig. 9A revealed significant removal percentage of 80.3% after four adsorption cycles. Adsorption efficiency undergoes a slight decline from the first cycle (97.3%) to the fourth cycle (80.3%). In the last generation cycle, the removal efficiency was found to be (75%) which could be referred to the fill up of the pores and breaking the bonds between IC molecules and nano-biochar. The results after increasing number of reused cycles demonstrate the great adsorption capability of nano-biochar and pinpoint the irreversible loss of adsorption capacity and the stability of IC sorbed onto nMOSAB.

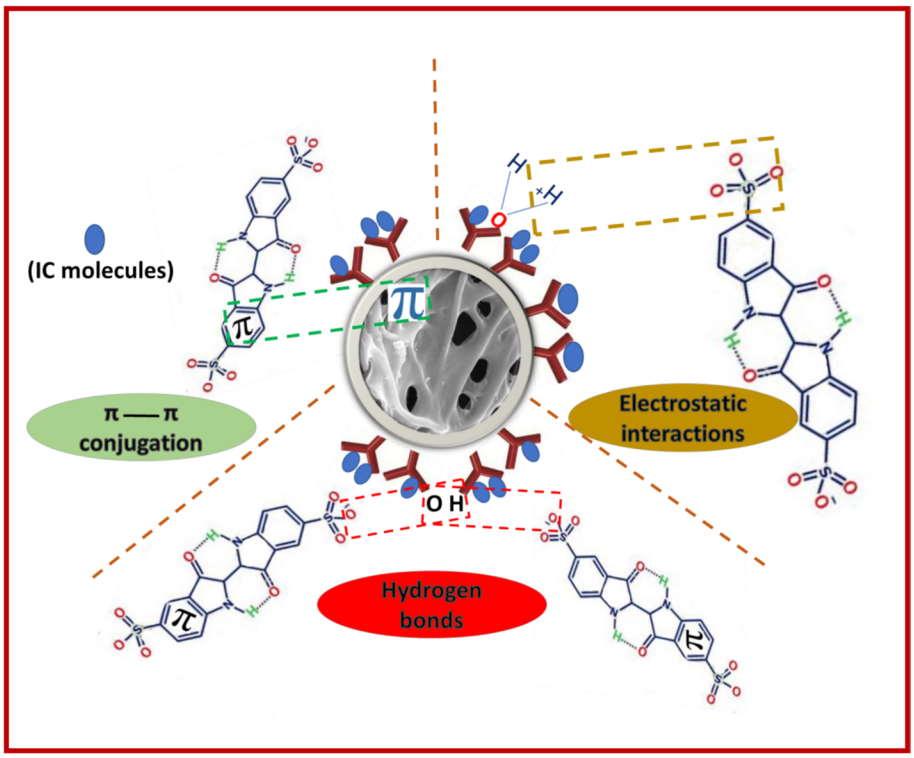

Fig. 8 The suggested mechanisms of IC adsorption by nMOSAB

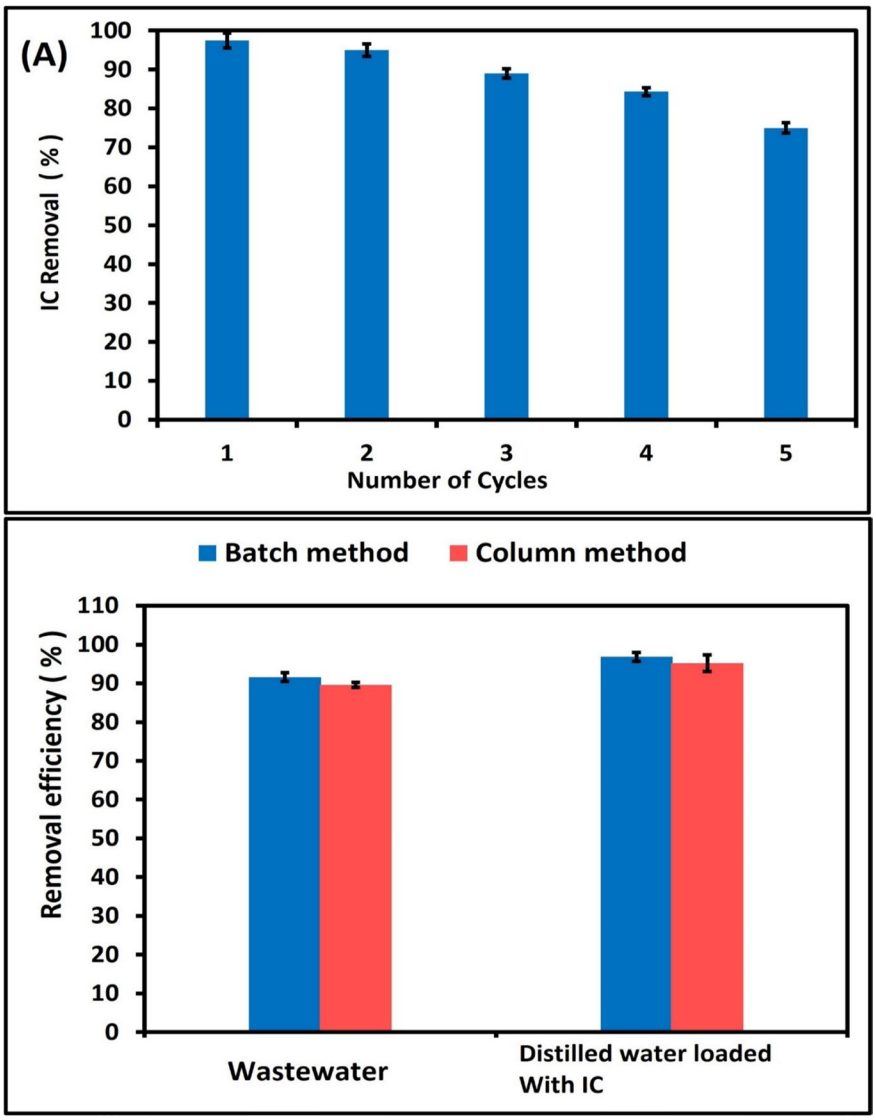

Fig. 9 **A** Removal efficiency of IC using nMOSAB after five adsorption–desorption cycles, **B** IC removal from environmental water samples by nMOSAB

IC removal from environmental water samples by nMOSAB

The capability of nano-biochar to remove indigo carmine from actual wastewater was assessed. Samples of wastewater contaminated with indigo carmine were obtained from a textile manufacturing facility located in Elboheira governorate, Egypt. The collected wastewater samples underwent filtration through Whatman cellulose microfiltration, which successfully eliminated impurities and solid particles, thereby facilitating a more precise evaluation of the wastewater's chemical characteristics. The chemical properties of the textile effluent are documented in Table 5. Dye concentration in textile wastewater was 32 mg L^{-1}. In addition, a dye solution having IC concentration of 30 mg L^{-1} was prepared. Two different adsorption systems were set up to conduct the adsorption tests. The first was a traditional batch experiment, and the second was through a packed-bed column. The

Table 5 Chemical characterization of the textile wastewater effluent

Analyte	Units	Values	Analyte	Units	Values
pH	–	7.32	IC	mg/L	32
EC	dS/m	1.20	Ca^{2+}	meq/L	2.7
TDS	mg/L	847	Mg^{2+}	meq/L	2.27
SAR	–	4.58	Na^{2+}	meq/L	7.22
Cd^{2+}	mg/L	0.02	K^{+}	meq/L	0.41
Zn^{2+}	mg/L	0.86	CO_3^{2-}	meq/L	0.00
Ni^{2+}	mg/L	0.19	HCO_3^{-}	meq/L	2.35
Pb^{2+}	mg/L	0.34	Cl^{-}	meq/L	5.52
Co^{2+}	mg/L	0.03	SO_4^{2-}	meq/L	4.42

EC electric conductivity, *TDS* total dissolved salts, *IC* indigo carmine dye, *SAR* Sodium adsorption ratio SAR $= \frac{Na^{+}}{\sqrt{\frac{Ca^{2+}+Mg^{2+}}{2}}}$

results obtained from both methods are shown in Fig. 8B. These findings demonstrate nMOSAB ability to absorb IC even in actual textile effluents.

Nano-biochar removal capability for IC elimination from textile wastewater in both batch and column methods was 91.6% and 89.6%, respectively. A slight decrease in previous results was noticed compared with removal percentage in solution with distilled water which was 96.8% and 95.2% for batch and column tests, respectively. This modest reduction could be due to the heterogeneous nature of textile effluents and existence of salts and other contaminants in the matrix of water causing a possibility for occurring interaction between different contaminants leading to limitation in the efficiency of sorbent (El-Kammah et al. 2022a).

Further studies should focus on evaluating the removal capacity of nMOSAB on the limitation of a wide variety of different pollutants including organic and inorganic pollutants, especially different species of dyes. The practical application of nMOSAB should have more attention in future research. Long-term stability of nMOSAB could be evaluated for achieving high adsorption efficiency. The examination of environmental concerns should include the verification of environmental safety and the assessment of the leaching process of pollutants from regenerated particles. It is crucial to investigate nMOSAB alongside other adsorbents or treatment techniques to evaluate its efficacy in adsorbing a range of pollutants from wastewater.

Conclusion

The current study examined the efficacy of nano-biochar derived from *Moringa oleifera* seeds (nMOSAB) in the removal of indigo carmine (IC). The investigation was conducted under optimal conditions, specifically at a pH of 4, contact duration of 90 min, and an adsorbent dosage of 100 mg of nMOSAB. The results indicated that nMOSAB attained an impressive removal rate of 97.5% for the elimination of IC from wastewater. The maximum adsorption capacity of IC on nanostructured MOSAB was determined to be 344.8 mg g^{-1} which represents a 9.5-fold enhancement in comparison with bulk MOS. This increase is ascribed to the augmented specific surface area and pore volume. Furthermore, the presence of reactive functional groups, including OH and C–H, in conjunction with the high porosity of the biochar's structure, plays a crucial role in enhancing the adsorption capacity of the nano-biochar.

The adsorption process occurred spontaneously and was exothermic, as it released heat throughout the reaction. The strong correlation of the experimental data with both the pseudo-second-order and power function models indicated that these models provide superior kinetic representations in comparison with other kinetic models. The major sorption mechanism in IC adsorption procedures onto nMOSAB was electrostatic interaction, π–π electron interaction and hydrogen bridge bond. Regeneration tests affirmed the efficient use of nMOSAB up to four cycles and its superiority in remediating IC-polluted solutions. This approach presents a novel and efficient perspective for its application in elimination of IC from wastewater. However, this study does have specific limitations, particularly regarding the possible influences of coexisting impurities on adsorption behavior, an area that has not been extensively explored. Furthermore, the research primarily concentrated on the adsorption of indigo carmine, with minimal investigation into other organic pollutants. Consequently, it is essential to conduct further applications to validate the broader applicability of this approach in wastewater treatment.

Supplementary Information The online version contains supplementary material available at https://doi.org/10.1007/s13201-025-02556-5.

Author contribution ME-K contributed to investigation, methodology, analysis, and writing—original draft. EE-K contributed to intellectual input, supervision, validation, and writing—review and editing. MM contributed to methodology, contribution, and validation.

Funding Open access funding provided by The Science, Technology & Innovation Funding Authority (STDF) in cooperation with The Egyptian Knowledge Bank (EKB).

Declarations

Conflict of interest On behalf of all authors, the corresponding author states that there is no conflict of interest and they have no known competing financial interests or personal relationships that could have appeared to influence the work reported in this paper.

Ethical approval This article does not contain any studies involving human participants performed by any of the authors.

References

Abbey CYB, Duwiejuah AB, Quianoo AK (2023) Removal of toxic metals from aqueous phase using cacao pod husk biochar in the era of green chemistry. Appl Water Sci 13:57

Akhtar M, Hasany SM, Bhanger MI, Iqbal S (2007) Sorption potential of *Moringa oleifera* pods for the removal of organic pollutants from aqueous solutions. J Hazard Mater 141:546–556

Araújo CST, Alves VN, Rezende HC et al (2010) Characterization and use of Moringa oleifera seeds as biosorbent for removing metal ions from aqueous effluents. Water Sci Technol 62:2198–2203

Araújo CST, Carvalho DC, Rezende HC et al (2013) Bioremediation of waters contaminated with heavy metals using *Moringa oleifera* seeds as biosorbent. Appl Bioremediation-Active Passive Approaches 23:227–255

Bagheri A, Abu-Danso E, Iqbal J, Bhatnagar A (2020) Modified biochar from *Moringa* seed powder for the removal of diclofenac from aqueous solution. Environ Sci Pollut Res 27:7318–7327

Bayram O, Koksal E, Moral E, et al (2022) Efficient Decolorization of Anionic Dye (Methyl Blue) by Natural-Based Biosorbent (nano-Magnetic Sophora Japonica Fruit Seed Biochar). Eurasia Proc Sci Technol Eng Math 17:69–82

Behera M, Nayak J, Banerjee S et al (2021) A review on the treatment of textile industry waste effluents towards the development of efficient mitigation strategy: an integrated system design approach. J Environ Chem Eng 9:105277

Bello OS, Adegoke KA, Akinyunni OO (2017) Preparation and characterization of a novel adsorbent from *Moringa oleifera* leaf. Appl Water Sci 7:1295–1305

Beltrán-Heredia J, Sánchez-Martín J (2008) Heavy metals removal from surface water with *Moringa oleifera* seed extract as flocculant agent. Fresenius Environ Bull 17:2134–2140

Beltrán-Heredia J, Sánchez-Martín J, Delgado-Regalado A (2009) Removal of carmine indigo dye with *Moringa oleifera* seed extract. Ind Eng Chem Res 48:6512–6520

Blanco SPDM, Scheufele FB, Módenes AN et al (2017) Kinetic, equilibrium and thermodynamic phenomenological modeling of reactive dye adsorption onto polymeric adsorbent. Chem Eng J 307:466–475

Chaari I, Fakhfakh E, Medhioub M, Jamoussi F (2019) Comparative study on adsorption of cationic and anionic dyes by smectite rich natural clays. J Mol Struct 1179:672–677

Choi K-Y (2021) Discoloration of indigo dyes by eco-friendly biocatalysts. Dye Pigment 184:108749

da Silva PMM, Camparotto NG, Lira KTG et al (2020) Adsorptive removal of basic dye onto sustainable chitosan beads: equilibrium, kinetics, stability, continuous-mode adsorption and mechanism. Sustain Chem Pharm 18:100318

Dai L, Zhu W, He L et al (2018) Calcium-rich biochar from crab shell: an unexpected super adsorbent for dye removal. Bioresour Technol 267:510–516

Dalaran M, Emik S, Güçlü G, et al (2011) Study on a novel polyampholyte nanocomposite superabsorbent hydrogels: Synthesis, characterization and investigation of removal of indigo carmine from aqueous solution. Desalination 279:170–182. https://doi.org/10.1016/j.desal.2011.06.004

Das N, Jana RK (2006) Adsorption of some bivalent heavy metal ions from aqueous solutions by manganese nodule leached residues. J Colloid Interface Sci 293:253–262

de Oliveira Brito SM, Andrade HMC, Soares LF, de Azevedo RP (2010) Brazil nut shells as a new biosorbent to remove methylene blue and indigo carmine from aqueous solutions. J Hazard Mater 174:84–92

Dey AK, Dey A, Goswami R (2022) Adsorption characteristics of methyl red dye by Na_2CO_3-treated jute fibre using multi-criteria decision making approach. Appl Water Sci 12:179

Elamin MR, Abdulkhair BY, Elzupir AO (2023) Removal of ciprofloxacin and indigo carmine from water by carbon nanotubes fabricated from a low-cost precursor: Solution parameters and recyclability. Ain Shams Eng J 14:101844. https://doi.org/10.1016/j.asej.2022.101844

El-Kammah M, Elkhatib E, Gouveia S et al (2022) Cost-effective eco-friendly nanoparticles for rapid and efficient indigo carmine dye removal from wastewater: adsorption equilibrium, kinetics and mechanism. Environ Technol Innov. https://doi.org/10.1016/j.eti.2022.102595

El-Kammah M, Elkhatib E, Gouveia S et al (2022b) Enhanced removal of indigo carmine dye from textile effluent using green cost-efficient nanomaterial: adsorption, kinetics, thermodynamics and mechanisms. Sustain Chem Pharm 29:100753. https://doi.org/10.1016/j.scp.2022.100753

El-Maghrabi N, Fawzy M, El Din MA (2024) Elimination of Cd^{2+} from synthetic and real polluted water by optimized *Acacia nilotica* biographene. Appl Water Sci 14:230

Elkhatib EA, Mahdy AM, ElManeah MM (2013) Effects of drinking water treatment residuals on nickel retention in soils: a macroscopic and thermodynamic study. J Soils Sediments 13:94–105

Elkhatib EA, Mahdy AM, Salama KA (2015) Green synthesis of nanoparticles by milling residues of water treatment. Environ Chem Lett 13:333–339

Elkhatib E, Moharem M, Mahdy A, Mesalem M (2017) Sorption, release and forms of mercury in contaminated soils stabilized with water treatment residual nanoparticles. Land Degrad Dev 28:752–761

Elkhatib EA, Moharem ML, Saad AF, Abdelhamed S (2024) A novel nanocomposite-based zeolite for efficient remediation of Cd-contaminated industrial wastewater. Appl Water Sci 14:75. https://doi.org/10.1007/s13201-024-02123-4

Feng N, Guo X, Liang S et al (2011) Biosorption of heavy metals from aqueous solutions by chemically modified orange peel. J Hazard Mater 185:49–54

Ferreira RM, de Oliveira NM, Lima LLS et al (2019) Adsorption of indigo carmine on Pistia stratiotes dry biomass chemically modified. Environ Sci Pollut Res 26:28614–28621

Fito J, Abewaa M, Nkambule T (2023) Magnetite-impregnated biochar of parthenium hysterophorus for adsorption of Cr (VI) from tannery industrial wastewater. Appl Water Sci 13:78. https://doi.org/10.1007/s13201-023-01880-y

Gadekar MR, Ahammed MM (2020) Use of water treatment residuals for colour removal from real textile dye wastewater. Appl Water Sci 10:1–8

Gallego-Ramírez C, Chica E, Rubio-Clemente A (2024) Elimination of indigo carmine in water by *Pinus patula* biochar: adsorption process optimization, kinetics and isotherms. J Environ Chem Eng 12:112425. https://doi.org/10.1016/j.jece.2024.112425

Gupta TB, Lataye DH (2017) Adsorption of indigo carmine dye onto acacia nilotica (babool) sawdust activated carbon. J Hazard Toxic Radioact Waste 21:04017013

Gutiérrez-Segura E, Solache-Ríos M, Colín-Cruz A (2009) Sorption of indigo carmine by a Fe-zeolitic tuff and carbonaceous material from pyrolyzed sewage sludge. J Hazard Mater 170:1227–1235

Harrache Z, Abbas M, Aksil T, Trari M (2019) Thermodynamic and kinetics studies on adsorption of Indigo Carmine from aqueous solution by activated carbon. Microchem J 144:180–189

Ho YS, Ng JCY, McKay G (2000) Kinetics of pollutant sorption by biosorbents. Sep Purif Methods 29:189–232

Hynes NRJ, Kumar JS, Kamyab H et al (2020) Modern enabling techniques and adsorbents based dye removal with sustainability concerns in textile industrial sector: a comprehensive review. J Clean Prod 272:122636

Jamil S, Afzal R, Khan SR et al (2024) Photocatalytic degradation of indigo carmine dye by hydrothermally synthesized graphene nanodots (GNDs): investigation of kinetics and thermodynamics. RSC Adv 14:23973–23986. https://doi.org/10.1039/D4RA02476A

Jindo K, Mizumoto H, Sawada Y et al (2014) Physical and chemical characterization of biochars derived from different agricultural residues. Biogeosciences 11:6613–6621

Keerthana Devi P, Geethakarthi A (2022) Arsenic removal using calcium hydroxyapatite synthesized from paper mill sludge. Appl Water Sci 12:174

Kekes T, Tzia C (2020) Adsorption of indigo carmine on functional chitosan and β-cyclodextrin/chitosan beads: equilibrium, kinetics and mechanism studies. J Environ Manage 262:110372

Kosmulski M (2009) pH-dependent surface charging and points of zero charge. IV. Update and new approach. J Colloid Interface Sci 337:439–448

Lehmann J, Joseph S (2015) Biochar for environmental management: science, technology and implementation. Routledge

Li Z, Hanafy H, Zhang L et al (2020) Adsorption of congo red and methylene blue dyes on an ashitaba waste and a walnut shell-based activated carbon from aqueous solutions: experiments, characterization and physical interpretations. Chem Eng J 388:124263

Li M, Wang H, Wu S, et al (2012) Adsorption of hazardous dyes indigo carmine and acid red on nanofiber membranes. RSC Adv 2:900–907

Mariska S, Lin J-L, Tuyet TTA et al (2024) Adsorption of methyl blue, dichromate, and copper on ettringite under various pH values. Appl Water Sci 14:95. https://doi.org/10.1007/s13201-024-02161-y

Mashhadimoslem H, Safarzadeh M, Ghaemi A et al (2021) Biomass derived hierarchical porous carbon for high-performance O_2/N_2 adsorption; a new green self-activation approach. RSC Adv 11:36125–36142

Nodeh HR, Sereshti H (2016) Synthesis of magnetic graphene oxide doped with strontium titanium trioxide nanoparticles as a nanocomposite for the removal of antibiotics from aqueous media. RSC Adv 6:89953–89965

O'Connor D, Peng T, Zhang J et al (2018) Biochar application for the remediation of heavy metal polluted land: a review of in situ field trials. Sci Total Environ 619:815–826

Oyekanmi AA, Katibi KK, Omar RC et al (2024) A novel oil palm frond magnetic biochar for the efficient adsorption of crystal violet and sunset yellow dyes from aqueous solution: synthesis, kinetics, isotherm, mechanism and reusability studies. Appl Water Sci 14:13

Rubangakene NO, Elwardany A, Fujii M, et al (2023) Biosorption of Congo Red dye from aqueous solutions using pristine biochar and ZnO biochar from green pea peels. Chem Eng Res Des 189:636–651. https://doi.org/10.1016/j.cherd.2022.12.003

Sahnoun AY, Selatnia A, Mitu L et al (2024) Basic Red 46 adsorption studies onto pyrolyzed by-product biomass. Appl Water Sci 14:111

Sambo GN, Adeola AO, Muhammad SA (2024) Oil palm waste-derived adsorbents for the sequestration of selected polycyclic aromatic hydrocarbon in contaminated aqueous medium. Appl Water Sci 14:113

Saxena M, Sharma N, Saxena R (2020) Highly efficient and rapid removal of a toxic dye: adsorption kinetics, isotherm, and mechanism studies on functionalized multiwalled carbon nanotubes. Surf Interfaces 21:100639. https://doi.org/10.1016/j.surfin.2020.100639

Shaikh WA, Chakraborty S, Islam RU (2020) Photocatalytic degradation of rhodamine B under UV irradiation using *Shorea robusta* leaf extract-mediated bio-synthesized silver nanoparticles. Int J Environ Sci Technol 17:2059–2072

Shaikh WA, Islam RU, Chakraborty S (2021) Stable silver nanoparticle doped mesoporous biochar-based nanocomposite for efficient removal of toxic dyes. J Environ Chem Eng 9:104982. https://doi.org/10.1016/j.jece.2020.104982

Shakoor MB, Ali S, Rizwan M et al (2020) A review of biochar-based sorbents for separation of heavy metals from water. Int J Phytoremediation 22:111–126

Sikdar D, Goswami S, Das P (2020) Activated carbonaceous materials from tea waste and its removal capacity of indigo carmine present in solution: synthesis, batch and optimization study. Sustain Environ Res 30:1–16

Singh H, Choden S (2016) Comparison of adsorption behaviour and kinetic modeling of bio-waste materials using basic dye as adsorbate. Indian J Chem Technol 21:359–367

Sun H, Lin Y, Takeshi H et al (2021) Synthesis of 3D graphene-based materials and their applications for removing dyes and heavy metals. Environ Sci Pollut Res 28:52625–52650

Tabti C, Benmohammed A, Boukabcha N, et al (2022) Synthesis, structural characterization and theoretical NLO activity of N-(4-Acetyl-5-(4-(Nitro) Phenyl)-4, 5-Dihydro-1, 3,4-Thiadiazol-2-yl)-N-Phenyl Acetamide. Polycycl Aromat Compd pp 1–22

Ullah F, Ji G, Irfan M et al (2022) Adsorption performance and mechanism of cationic and anionic dyes by KOH activated biochar derived from medical waste pyrolysis. Environ Pollut 314:120271

Wang L, Chen L, Tsang DCW et al (2020a) Biochar as green additives in cement-based composites with carbon dioxide curing. J Clean Prod 258:120678. https://doi.org/10.1016/j.jclepro.2020.120678

Wang S, Kwak J-H, Islam MS et al (2020b) Biochar surface complexation and Ni(II), Cu(II), and Cd(II) adsorption in aqueous solutions depend on feedstock type. Sci Total Environ 712:136538

Zhang F, Tang X, Huang Y et al (2019) Competitive removal of Pb^{2+} and malachite green from water by magnetic phosphate nanocomposites. Water Res 150:442–451

Zhang X, Sun P, Wei K et al (2020) Enhanced H_2O_2 activation and sulfamethoxazole degradation by Fe-impregnated biochar. Chem Eng J 385:123921